

PROCESSES OF NONCONSUMABLE ELECTRODE WELDING WITH WELDING CURRENT MODULATION (Review).

Part II. Effects of arc impact on the metal being welded

BOYI WU¹ and I.V. KRIVTSUN²

¹Guangdong Institute of Welding (China-Ukraine E.O.Paton Institute of Welding)
363 Chiansin Str., 510650, Guangzhou, Tianhe. E-mail: wuby@gwi.gd.cn

²E.O. Paton Electric Welding Institute of the NAS of Ukraine
11 Kazymyr Malevych Str., 03150, Kyiv, Ukraine. E-mail: office@paton.kiev.ua

A review of studies, devoted to the processes of nonconsumable electrode inert-gas welding with welding current modulation was performed. The second part of the review is devoted to analysis of the works, dealing with the features of metal penetration (aluminium alloys, stainless steels, high-temperature nickel-chromium alloys) and weld formation in TIG welding with modulated current. 12 Ref., 16 Tables, 19 Figures.

Keywords: arc with refractory cathode, TIG welding, metal being welded, penetration, weld, welding current modulation, pulse, frequency, fill factor, amplitude

Features of burning of a nonstationary arc in nonconsumable electrode welding with current modulation, described in the first part of this review [1], cause considerable changes of the characteristics of thermal and dynamic impact of the arc on the metal being welded, and, therefore, of the processes of its penetration and formation of welds compared to the respective processes at DC TIG welding.

Work [2] is one of the first studies, devoted to comparative analysis of the quality and mechanical properties of welds, made at single-pass TIG welding of samples from aluminium alloy 2219 of thickness of 0.125; 0.250; 0.350 in. (3.2; 6.4 and 8.9 mm) at SPDC and with pulse modulation of current. Two power sources were used during the experiments: for high-frequency (HFP) and low-frequency (LFP) pulse modulation of welding current. The first of them ensured HFP modulation of current by rectangular pulses up to values of 500 A, with pulse repetition rate $f = 2\text{--}25$ kHz and adjustable fill factor δ in the range from 20 up to 80 %, that allowed variation of average current value from 100 up to 400 A. The second source ensured additional LFP modulation of high-frequency arc current by rectangular pulses with the frequency of 1–10 Hz and fill factor from 10 up to 100 %. The base current was equal to 3 A in all the cases. It should be noted that in addition to feeding single-polarity current pulses, such a system also allows realization of welding current modulation (including combined one) by pulses of straight and reverse polarity.

Overlay and butt welds (in the downhand position, unsupported) were made on all the samples in two modes of current modulation: high-frequency and combined (high-frequency + low-frequency modulation), as well as at DC TIG welding. Produced welds were subjected to radiographic inspection. X-ray images were analyzed at tenfold magnification and the number of defects (pores and oxide inclusions) of more than 0.005 in. (0.13 mm) size was determined along the entire weld length. Figures 1, 2 show the dependencies of the length of discontinuities (defects) on the length of welds on samples from aluminium alloy 2219 8.9 and 3.2 mm thick, respectively, at different modulation modes. Experimental data given in these figures are indicative of the fact that application of HFP modulation of current essentially (up to 80 %) lowers the number of pores and nonmetallic inclusions per a unit of weld length, whereas appli-

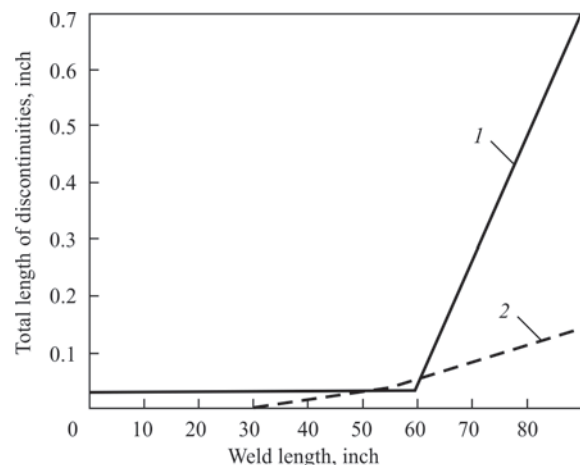


Figure 1. Total length of discontinuities (inches), depending on weld length (inches) in TIG welding of samples 8.9 mm thick at direct current (1) and with HFP modulation of current (2) [2]

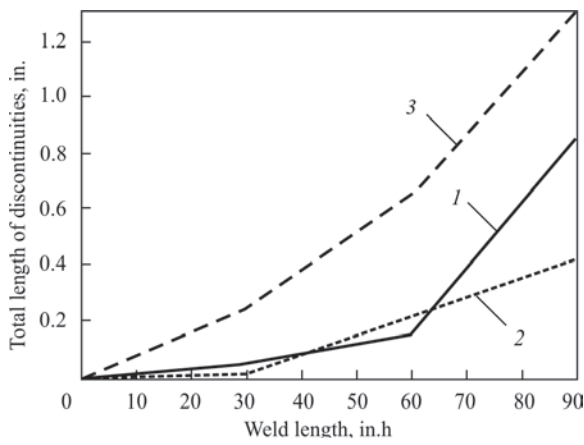


Figure 2. Total length of discontinuities, depending on weld length at TIG welding of samples 3.2 mm thick at direct current (1), with HFP modulation of current (2) and with combined modulation (3) [2]

application of the combined mode markedly impairs this characteristic.

The author of [2] showed that high-frequency pulse modulation of welding current can also be effectively used for destruction of nonuniform cast structure of metal found in welds made by nonconsumable electrode DC welding. As a result, the microstructure of weld metal in welding aluminium alloy 2219 with HFP modulation of current is homogeneous both in the longitudinal and transverse section of the weld. Therefore, such welds are characterized by 10–15 % higher fracture values than in DC TIG welding.

Low-frequency modulation of arc current in combination with high-frequency modulation does not lead to formation of a homogeneous microstructure in welds on aluminium alloy 2219. It can be used only to control the weld geometry in single-pass TIG welding of samples of 0.125 in. (3.2 mm) thickness with free formation. This allows performing quality welding of thinner materials that ensures reduction of welded structure weight.

Work [3] presents experimental studies of the impact of five parameters of the mode of TIG welding of stainless steel samples with low-frequency (1–5 Hz) modulation of current by rectangular pulses, namely: amplitude (depth) and frequency of current modulation, fill factor and maximum current depth value, as well as welding speed on penetration depth, weld form

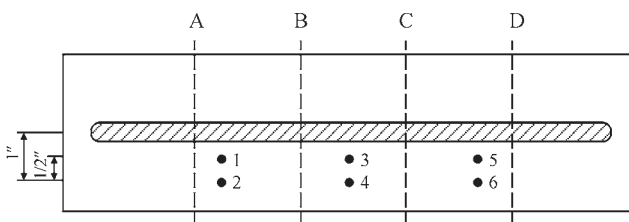


Figure 3. Arrangement of thermocouples on sample surface, points 1, 3, 5 at the distance of 1/2 in. (12.7 mm); 2, 4, 6 — 1 in. (25.4 mm) from weld center line [3]

Table 1. Parameters of the studied welding modes [3]

Parameter	Values		
Depth of current modulation I_L/I_H , %	80	50	20
Modulation frequency f , Hz	5	3	1
Fill factor δ , %	75	50	25
Maximum current value I_H , A	175	125	75
Welding speed S , in./min	9	6	3

factor and thermocycles in the metal being welded. In order to analyze such an impact, 46 combinations were selected on three levels of the above parameter values, given in Table 1, by the method of mathematical planning of the experiment, for which full-scale experiments were performed.

All the experiments were performed with application of water-cooled welding torch with a refractory cathode from thoriated tungsten of 3/32 in. (2.38 mm) diameter, arc length was set equal to 0.05 in. (1.27 mm) and a mixture of 75 % He + 25 % Ar was used as shielding gas. Overlay welds were made on samples of stainless steel 304 of 1/4 in. (6.35 mm) thickness, the length of all the welds was the same and equal to 10 in. (25.4 cm). Temperature was measured by chromel-alumel thermocouples in six points on the sample surface, shown in Figure 3.

Characteristic time dependencies of temperature in the respective points are shown in Figure 4. Maximum temperature values in points 1, 3, 5, as well as in points 2, 4, 6 turn out to be practically the same.

Measured values of maximum temperature in the selected points were correlated with the rate of energy input X (J/in.) of the welding process. In the case of pulse modulation of current it was calculated as follows $X = 0.6U[I_H\delta + I_L(100 - \delta)]/S$, where U is the arc voltage, which was selected constant (independent on pause current and maximum current values) and equal to 11.75 V, and designations of the other parameters and their dimensions correspond to those used in Table 1. The given in Figure 5 dependencies

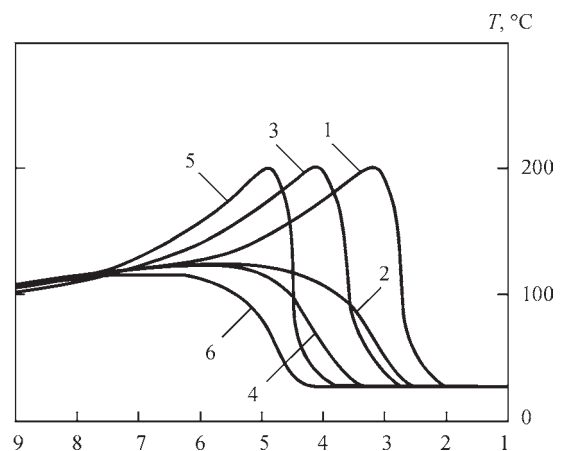


Figure 4. Thermal cycles in different points of sample surface [3]

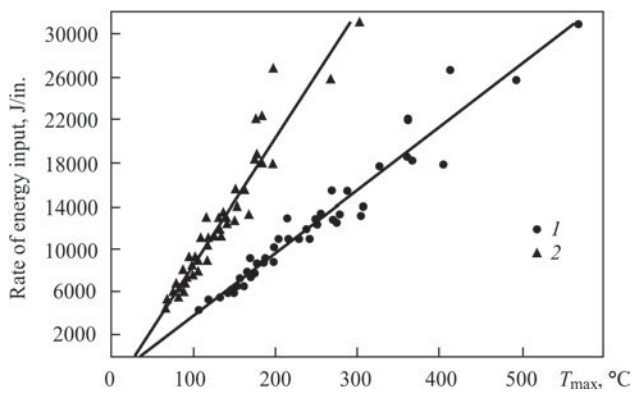


Figure 5. Dependence of maximum temperature values on the rate of energy input in points located at distance 1/2 in. from the weld center line (1) and in points located at 1 in. distance (2) [3] of maximum temperature values in points 1, 3, 5 and 2, 4, 6, respectively, on the rate of energy input of the process are indicative of linear nature of the above dependencies in the entire studied range of welding mode parameters.

Obtained experimental data were the base for plotting the regression equations for calculation of penetration depth h and its ratio to weld width h/b , as functions of the considered parameters of the welding mode. Regression equation proposed by the authors for determination of the penetration depth, shows that the main role here is played by welding speed S , followed by modulation amplitude I_L/I_H and maximum current value I_H , then fill factor δ , and finally, frequency f . Lines of constant penetration depth h in $S - I_H$ variables plotted using this equation, are shown in Figure 6. The same Figure shows the lines of constant values of the rate of energy input X , calculated as indicated above. As regards the regression equation for calculation of the ratio of penetration depth to weld width, the main role here is played by maximum current value I_H , followed by welding speed S , then modulation amplitude I_L/I_H , frequency f and fill factor δ .

Calculated data given in Figure 6, allow, for instance, determination of optimum combinations of I_H and S , corresponding to minimum rate of energy input, required for achieving any specified penetration depth. In particular, the best combination of the above parameters of the welding mode to achieve the penetration depth $h = 0.09$ in. (2.29 mm) is $I_H = 115$ A, $S = 6$ in./min, minimum required value X being equal to about 10 kJ/in.

This approach was used to analyze 27 combinations of welding mode parameters. Obtained data for DC TIG welding, as well as at three combinations of values of fill factor δ and modulation amplitude I_L/I_H are shown in Figure 7.

Finishing consideration of work [3], we should note an important conclusion, reached by the authors, namely at any combinations of mode parameters of

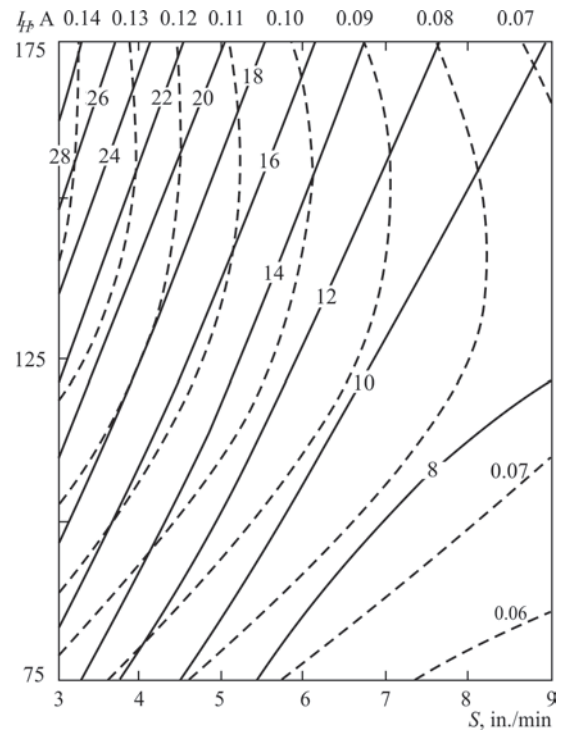


Figure 6. Lines of constant values of penetration depth (dash curves, numbers indicate h values in inches) and rate of energy input (solid curves, numbers indicate X values, kJ/in.) at $\delta = 75\%$; $I_L/I_H = 20\%$; $f = 1$ Hz [3]

TIG welding with LFP modulation of current the penetration depth and its ratio to weld width turn out to be greater than in the case of DC welding, at the same rate of energy input.

Work [4] is devoted to experimental studies of the processes of TIG welding and plasma welding using low-frequency (1–40 Hz) and high-frequency (2–20 kHz) pulse modulation of welding current, as well as combined modulation (10 Hz + 2 kHz). All the experiments on TIG welding were performed using a torch with tungsten (W + 2 % Th) cathode of 3/32 in. (2.36 mm) diameter, with 60 deg sharpening

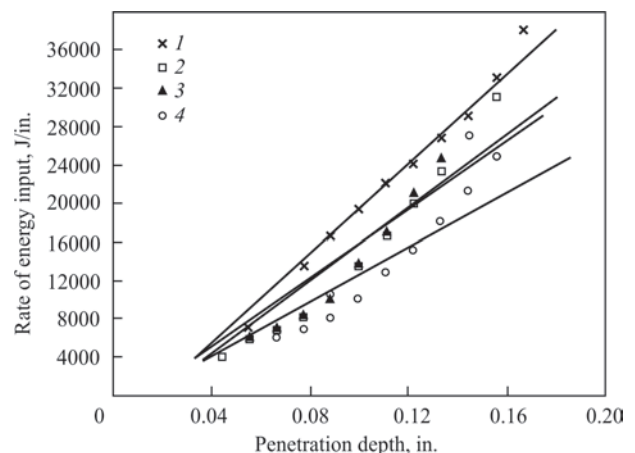


Figure 7. Minimum possible values of the rate of energy input of the process of TIG welding of stainless steel, depending on achieved penetration depth for welding at direct current (1) and three modes with pulse modulation of arc current: $\delta = 50\%$, $I_L/I_H = 80\%$ (2); 25 % and 80 % (3); 75 % and 20 % (4) [3]

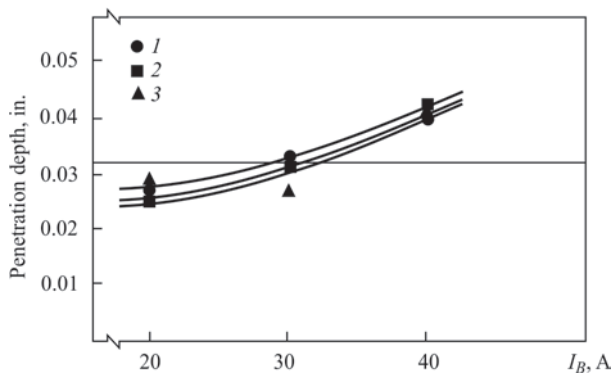


Figure 8. Dependence of penetration depth on pause current at current modulation by rectangular pulses in the form of a meander with repetition rate $f = 2$ (1); 10 (2) and 20 (3) kHz and average current value $I_{av} = 60$ A; horizontal line shows the penetration depth in TIG welding at direct current $I = 60$ A [4]

angle of the electrode working end, arc length was set equal to 3/32 in. (2.36 mm), and argon was used as shielding gas. Welding of samples from Inconel 600 alloy of 0.109 in. (2.77 mm) thickness was performed, welding speed was set constant, equal to 4 inches per minute (1.69 mm/s). The arc was powered from two sources, one of which was designed for low-frequency modulation of current, and the second, transistor source was used for high-frequency modulation.

As the results of studying the impact of low-frequency pulse modulation of welding current on the depth and shape of metal penetration are described above (see work [13]), we will consider the data of [4], concerning TIG welding with high-frequency pulse modulation of arc current. For correct comparison of penetration depth h at direct current with its value in the case of HFP modulation of arc current by rectangular pulses, the respective experiments were conducted at the same value of average current $I_{av} = \frac{I_B t_B + I_P t_P}{t_B + t_P}$, where I_B, I_P are the values of current in the pause and in the pulse; t_B, t_P are the durations of the pause and pulse, respectively. Figure 8 gives the dependencies of value h on current

in the pause in TIG welding with current modulation in the form of a meander $\left(\frac{t_P}{t_B} = 1\right)$ at modulation frequencies

$$f = \frac{1}{t_B + t_P}$$

equal to 2, 10 and 20 kHz and average current $I_{av} = 60$ A. Horizontal line shows the depth of metal penetration in welding at direct current equal to I_{av} . As follows from experimental data given in this Figure, the penetration depth in TIG welding with HFP modulation of arc current depends weakly on modulation frequency, rises noticeably with I_B increase, and at $I_B > 30$ A exceeds the respective value for DC welding.

In work [4] metallographic investigations of the metal of weld and HAZ were performed, in order to study the influence of current modulation parameters on weld microstructure. In particular, it was established that with increase of modulation frequency f of welding current, the size of metal penetration zone decreases, whereas the size of the HAZ becomes greater. This is indicative of lowering of the efficiency of melting of the metal being welded (thermal efficiency of the process) at f increase. As regards weld metal microstructure, application of HFP modulation of current does not lead to its marked improvement compared to DC TIG welding.

In work [5] studies of the impact of current modulation on penetration depth D and width W of the weld face in welding samples from stainless steel 304 were performed. In the case of sinusoidal modulation of current of 4 mm arc in the range of 30–270 A (average current $\langle I \rangle = 150$ A) dependencies of penetration depth and weld width on modulation frequency, shown in Figure 9, were obtained.

As follows from experimental data given in these Figures, the penetration depth in the case of welding by modulated current in the entire studied range of modulation frequencies turns out to be much higher,

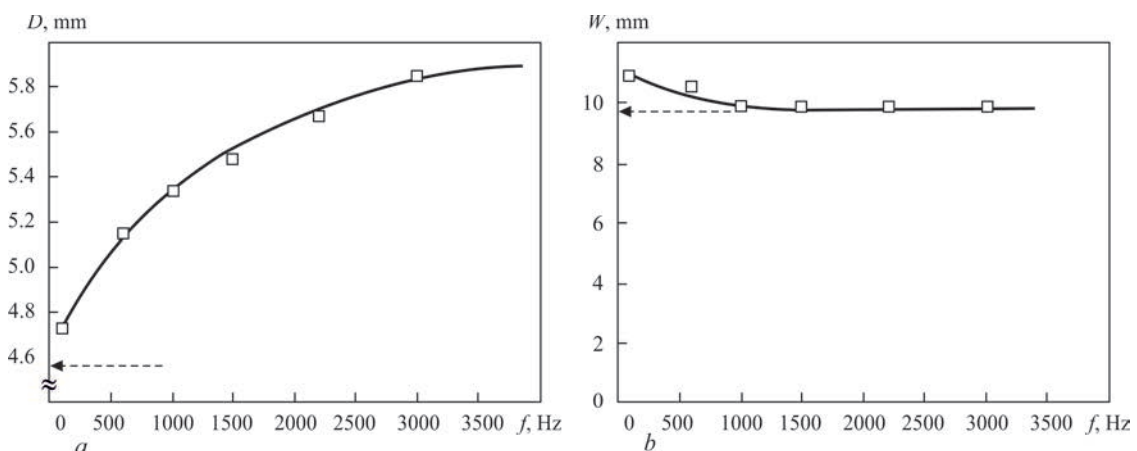


Figure 9. Dependencies of penetration depth (a) and width of weld face side (b) on frequency of sinusoidal modulation of current; dash lines show the respective values for welding at direct current $I = 150$ A [5]

than in the case of welding at direct current equal to average value of modulated current. Here value D rises monotonically with modulation frequency increase, reaching a plateau at frequencies of the order of 4 kHz. As regards weld width, in the case of welding with low-frequency current modulation ($f = 100$ Hz), it turns out to be somewhat higher than the respective value for DC welding, decreasing with increase of modulation frequency and reaching a constant value, corresponding to W value at DC welding, at frequency of the order of 1.5 kHz.

Work [6] also gives the data which are indicative of greater penetration depth at application of high-frequency modulation of arc current. In particular, Figure 10 shows the dependence of penetration depth T_N on pulse current I_p (curve 1) at modulation frequency of 10 kHz, pulse current $I_B = 5$ A, and constant average arc current equal to 50 A (current modulation was performed by rectangular pulses, fill factor was selected from the condition of constant value of average current). The same Figure gives the dependencies of T_N on arc length at TIG welding at modulated current with modulation frequency of 10 kHz and average current $\langle I \rangle = 50$ A (curve 2), as well as in welding at direct current (curve 3) equal to average value of modulated current.

As follows from Figure 10, the penetration depth increases with increase of current modulation amplitude (see curve 1) and decreases markedly at increase of arc length (see curves 2, 3), while remaining considerably higher than in the case of current modulation with 10 kHz frequency compared to DC welding.

In addition, work [6] gives the images of cross-sections of welds, made by TIG welding (95 % Ar + 5 % H was shielding gas, without filler wire) of stainless steel 1.4301 (AISI 304) 2 mm thick at direct current and with HFP modulation of arc current. As follows from comparison of photographs of butt weld cross-sections presented in Figure 11, application of HFP modulation of arc current allows achieving the

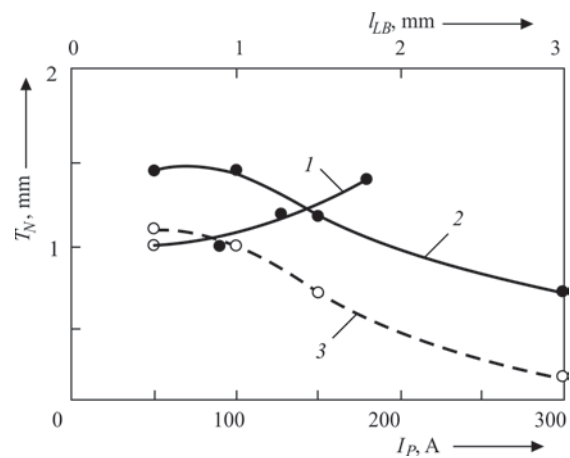


Figure 10. Dependencies of penetration depth T_N on pulse current I_p (1) and on arc length I_{LB} (2 — 10 kHz, 3 — 0 Hz) [6]

same result, as in the case of welding at direct current equal to average value of modulated current, at significantly higher welding speed. This is indicative of not only higher penetrability of modulated current arc, but also its higher spatial stability.

In [7], alongside the results of experimental studies of the characteristics of an arc with a refractory cathode and copper water-cooled anode at HFP modulation (up to 20 kHz) with high peak values of current (up to 500 A), data are given on the impact of such a modulation on penetration depth and width of overlay welds, made by TIG welding on samples of stainless steel 16 mm thick, also with application of filler wire of 0.6 mm diameter (chemical composition of the used materials is given in Table 2).

Figure 12 presents the dependencies of penetration depth D and weld width W on arc length L at TIG welding with HFP modulation of current (average and peak values of current of 150 and 500 A, respectively) and in welding at direct current, equal to average value of modulated current. As follows from experimental data given in this Figure, the width of welds at a short arc ($L = 0.5$ mm) is practically independent on modulation frequency. With increase of arc length at modulation frequency of 5 kHz, W value first

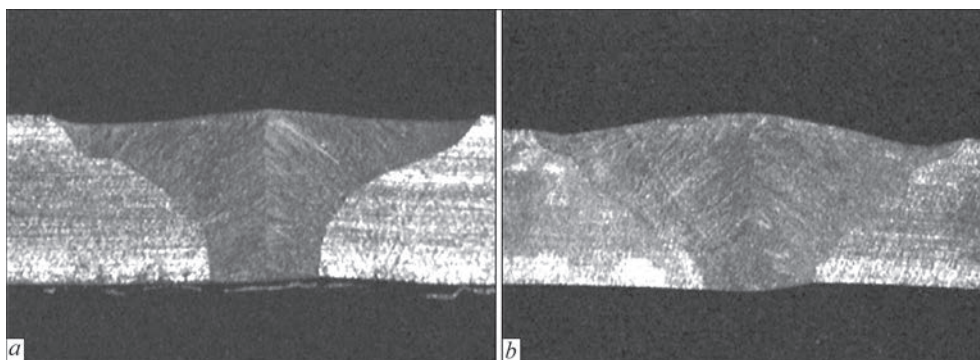


Figure 11. Transverse macrosections of butt welds made on steel 1.4301 2 mm thick by TIG welding with HFP modulation of current (a) and at direct current (b) at the following mode parameters: a — 6 kHz modulation frequency, 375 A pulse current, 292 A average current, 2.4 m/min welding speed; b — 292 A arc current; 1.6 m/min welding speed [6]

Table 2. Composition of metal being welded and filler wire [7]

Material	Composition, wt.%							
	C	Si	Mn	P	S	Ni	Cr	Fe
Metal	0.04	0.6	1.01	0.032	0.005	8.26	18.34	Bal.
Wire	0.013	0.35	1.88	0.024	0.003	12.65	19.63	Bal.

risers, then somewhat decreases and then rises again, reaching the maximum value of the order of 10 mm at $L = 3$ mm (see Figure 12, *a*). At frequencies of 10 and 16 kHz, W value rises nonmonotonically with increase of arc length. Note that in the case of modulated current welding the welds turn out to be noticeably wider, than in the case of DC welding at the same length of the arc.

As regards the penetration depth at TIG welding with HFP modulation of current at frequencies from 5 up to 16 kHz, value D decreases at increase of arc length faster in the range of $L = 0.5 - 1.0$ mm and more smoothly at $L > 1$ mm, while remaining markedly higher than the respective values for the case of DC welding (see Figure 12, *a*). In welding with application of filler wire, the above regularities of variation of values D and W are preserved with increase of arc length (see Figure 12).

Figure 13 shows the shapes of the cross-section of overlay welds made by TIG welding of stainless steel (see Table 2) with HFP modulation of current (average and peak current values of 150 and 500 A, respectively), as well as at direct current equal to average value of modulated current. Unfortunately, work [7] does not give any data on welding speed or

wire feed rate in the experiments, the results of which are presented in Figures 12, 13, and does not specify the length of the arc, at which the penetration shapes shown in Figure 13 were obtained, either.

Work [8] by Indian scientists is a study of the impact of low-frequency ($f = 6$ Hz) modulation of arc current at TIG welding of an aluminium alloy on temperature distribution in the welded metal and its penetration shape, strength properties and microstructural features of the metal of weld and HAZ, distribution of hardness and residual stresses in the welded samples. All the experiments were performed using an arc with a refractory cathode (W + 2 % Th) of 3.2 mm diameter, arc length was kept constant, equal to 2 mm, and chemically pure argon (99.99 %) was used as shielding gas. Overlay welds were made on 4 mm thick samples from aluminium alloy AA6351-T6, the composition and mechanical properties of which are given in Tables 3, 4. Temperature was measured by thermocouples located at distances of 5, 15 and 30 mm from the weld center line.

Parameters of the modes in the experiments on welding at direct current and with low-frequency pulse modulation of arc current are given in Tables 5 and 6, respectively. Speed s of modulated current

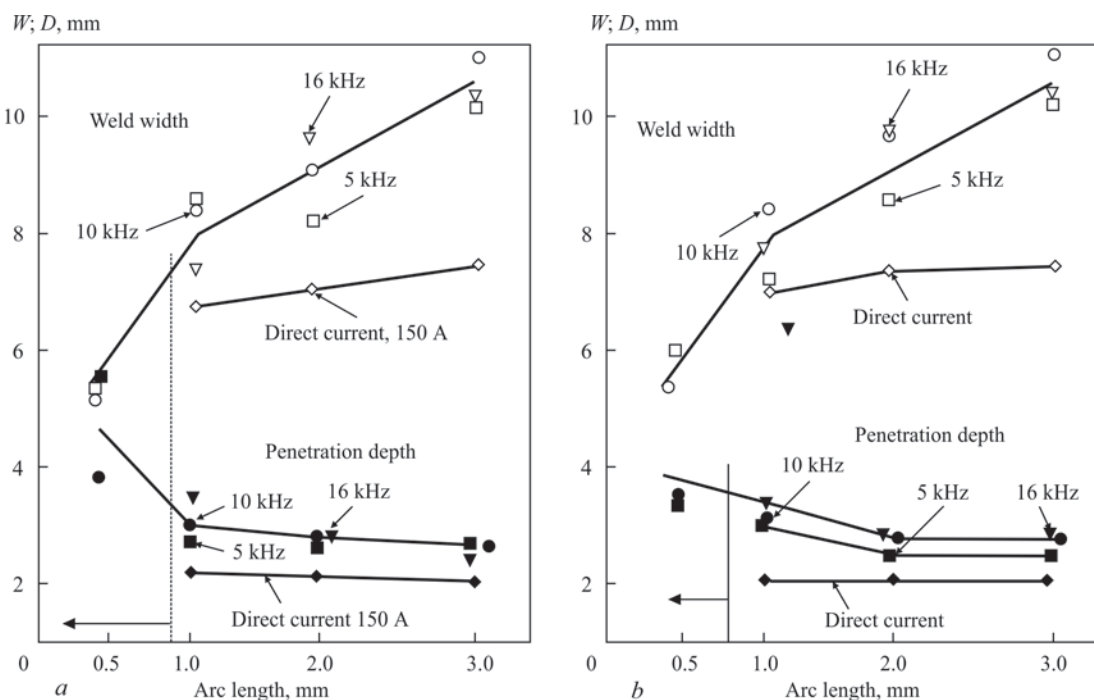


Figure 12. Dependencies of penetration depth and weld width on arc length in TIG welding with current modulation at frequencies of 5, 10 and 16 kHz (500 A peak current, 150 A average current) and in welding at direct current of 150 A: *a* — welding without filler; *b* — welding with filler wire; horizontal arrow shows the area in which DC welding cannot be performed [7]

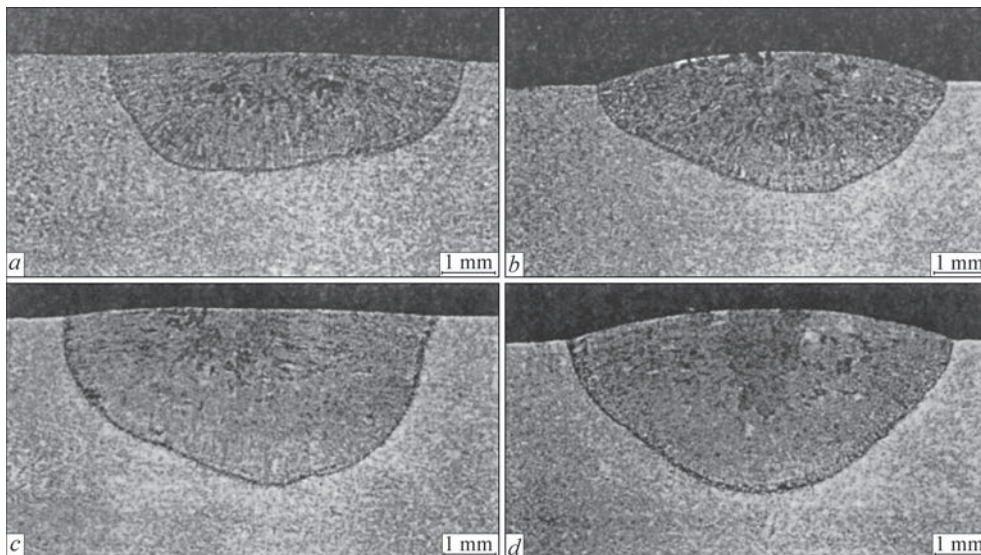


Figure 13. Transverse macrosections of overlay welds in TIG welding at direct current of 150 A, made without filler (a) and with filler wire (c), as well as at HFP modulation of welding current at 16 kHz frequency (500 A peak current, 150 A average current) without application (b) and with application (d) of filler wire [7]

welding was selected the same as at DC welding (4.167 mm/s), process efficiency η was assumed to be constant, equal to 70 %, and independent on the welding mode. The respective rate of energy input was calculated by formula $Q = (\eta IV)/s$, where I , V are the welding current and arc voltage. In the case of modulated current, its value, included into the given formula, was determined as mean $I_m = (I_p t_p + I_b t_b)/t_T$, where I_p , I_b are the current values in the pulse and in the pause; t_p , t_b are the pulse and pause durations; t_T is the duration of modulation period; fill factor was calculated as $\delta = t_p/t_T$.

The shape and geometrical dimensions of the cross-sections of overlay welds, obtained in the experiments on nonconsumable electrode welding at direct current (DC), and in welding by modulated current (MC) are given in Table 7. Here it should be noted that experiment No.5 on DC welding (rate of energy input of 312 J/mm) resulted in cracking, so that the respective data in work [8] are omitted.

Maximum values of temperature and values of cooling rate in the range of 400–200 °C, in points located at the distance of 5 and 15 mm from the weld center line, are given in Table 8.

Just two samples were used for comparison of the properties of strength, microhardness, microstructure

Table 3. Composition of metal being welded (wt.%) [8]

Mg	Si	Fe	Cu	Mn	Zn	Zr	Al
0.7	1.2	0.5	0.1	0.6	0.2	0.05	Bal.

Table 4. Mechanical properties of base metal [8]

Yield point, MPa	Ultimate strength, MPa	Elongation per 50 mm of length, %	Microhardness HV at 0.49 N
150	250	20	95

and residual stresses. On one of them the overlay weld was made by DC arc of 120 A (experiment No.2), and on the other the weld was made with welding current modulation at pulse current of 140 A (experiment No.4). Penetration depth was approximately the same in both the samples: 1.45 and 1.52 mm (see Table 7), that allowed comparing the strength properties of overlay welds by removing the unmelted metal down to sample thickness of 1.5 mm. Table 9 gives the results of the respective mechanical testing.

Microhardness distribution of the studied samples is given in Table 10, and Table 11 shows the distribution of residual stresses.

As follows from experimental data, given in Tables 9–11, application of LFP modulation of current ($f = 6$ Hz) leads to improvement of strength proper-

Table 5. Parameters of DC welding modes [8]

Experiment number	Welding current, A	Arc voltage, V	Welding speed, mm/s	Process efficiency, %	Rate of energy input, J/mm
1	110	12.5	4.167	70	231
2	120	12.7	4.167	70	256
3	130	12.2	4.167	70	266
4	140	12.5	4.167	70	294
5	150	12.4	4.167	70	312

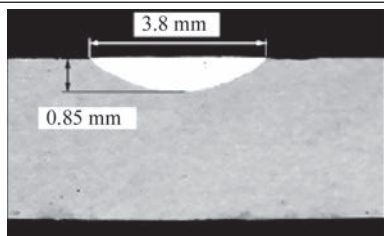
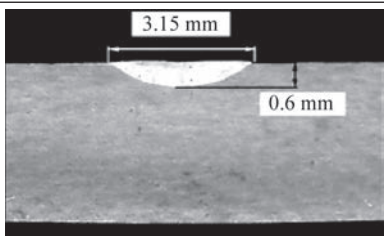
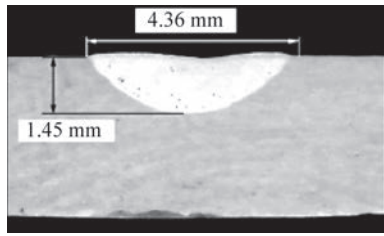
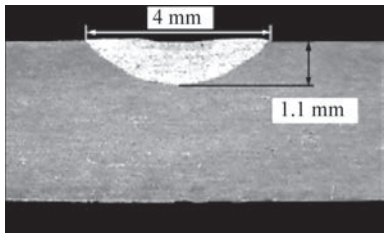
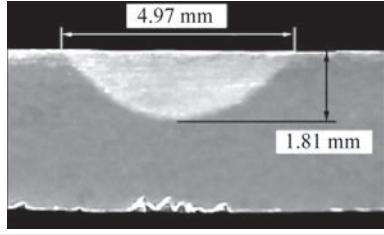
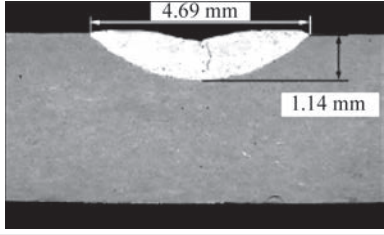
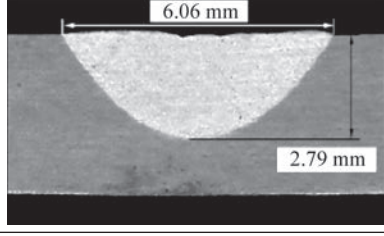
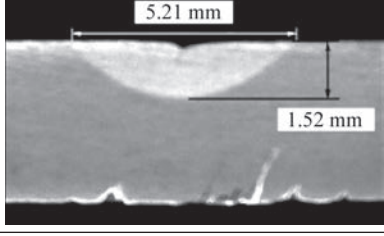
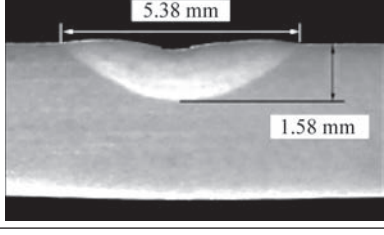
Table 6. Parameters of the modes of welding with pulse modulation of arc current ($f = 6$ Hz) [8]

Experiment number	Pulse current, A	Pause current, A	Arc voltage, V	Fill factor, %	Rate of energy input, J/mm
1	110	55	11	50	161
2	120	60	12	50	191
3	130	65	13	50	224
4	140	70	12.5	50	232
5	150	75	13.5	50	269

ties, increase of microhardness and lowering of the level of residual stresses in the samples, compared to those welded at direct current. This is caused by refinement of the structure of the metal of weld and HAZ at welding current modulation, found in [8].

Work [9] gives the experimental data on penetration depth and shape in TIG welding of stainless steel 0Cr18Ni9Ti 6 mm thick in argon (welding speed of 120 mm/min) with high-frequency ($f = 20-80$ kHz) modulation of current by rectangular pulses in the

Table 7. Cross-sectional shapes and geometry of welds made by TIG welding at direct current and low-frequency modulation of current [8]

Current, A	Weld cross-section		D/T*		W/D	
	DC	MC	DC	MC	DC	MC
110			0.22	0.15	5.50	5.25
120			0.36	0.28	3.00	3.64
130			0.45	0.29	2.75	4.11
140			0.70	0.38	2.17	3.43
150	–		–	0.40	–	3.41

*T is sample thickness.

Table 8. Maximum values of temperature and cooling rate in TIG welding at direct current, as well as with pulse modulation of arc current [8]

Experiment number	Current, A	Rate of energy input, J/mm		Maximum temperature (5 mm), K		Cooling rate, °C/s		Maximum temperature (15 mm), K	
		DC	MC	DC	MC	DC	MC	DC	MC
1	110	231	161	586	589	16.1	19.2	475	460
2	120	256	191	648	609	14.4	13.5	210	447
3	130	266	224	666	626	12.7	13.0	519	484
4	140	294	232	710	704	11.8	12.9	544	505
5	150	312	268	–	707	–	11.9	–	516

Table 9. Strength characteristics of welds made at direct current and with pulse modulation of current [8]

Process	Yield limit, MPa	Ultimate strength, MPa	Elongation, %	Strength relative to base metal, %
DC	185	200	8	80
MC	205	225	10	90

Table 10. Microhardness distribution in samples welded at direct current and with pulse modulation of current [8]

Process	Microhardness HV			
	Weld center	5 mm from weld center	15 mm from weld center	Base metal
DC	72	84	92	95
MC	81	88	93	95

Table 11. Distribution of residual stresses in samples welded at direct current and with pulse modulation of current [8]

Process	Residual stresses, MPa			
	Weld center	5 mm from weld center	15 mm from weld center	Base metal
DC	134	92	-60.5	-38.4
MC	112	74	-55.6	-36.3

form of a meander (pulse current of 130 A, pause current of 50 A). Given for comparison are the respective data for welding at direct current, the value of which is equal to effective value of modulated current ($I = I_{eff} \approx 100$ A). Macrosections of the respective overlay welds are shown in Table 12, and Figure 14 gives the dependencies of penetration depth H and weld width B on modulation frequency. As follows from the given data, the penetration depth rises nonmono-

tonically with frequency rise, and weld width decreases practically linearly.

The authors of [9] also performed numerical modeling of geometrical parameters of overlay welds, made in the experiments. Calculations were performed taking into account the deflection of weld pool surface, caused by the values of arc pressure on this surface, rising with frequency. Table 13 gives the re-

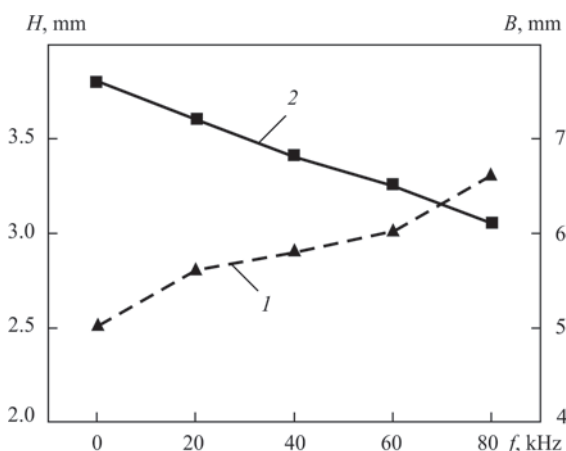


Figure 14. Dependencies of penetration depth (H) and weld width (B) on frequency of arc current modulation [9]

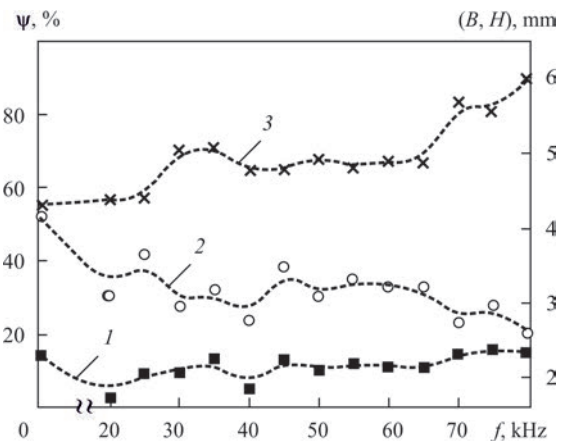


Figure 15. Dependencies of penetration depth H , mm (1), weld width B , mm (2) and weld form factor ψ , % (3) on frequency of welding current modulation [10]

Table 12. Cross-sectional shapes of overlay welds, made at direct current and with HFP modulation of current [9]

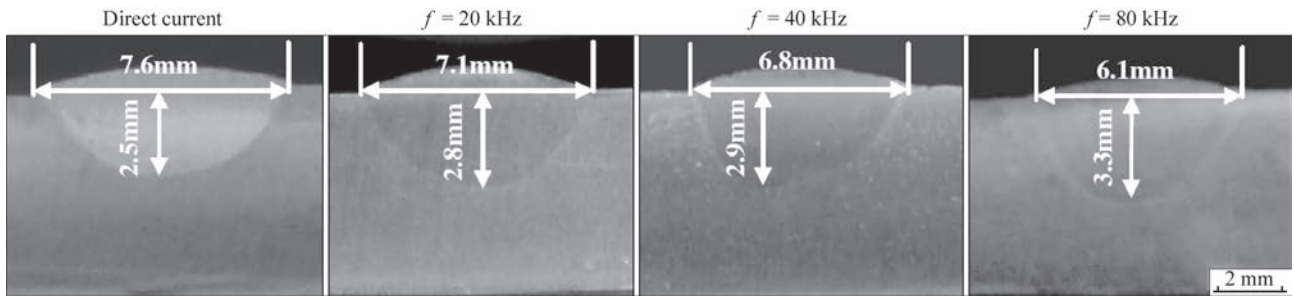


Table 13. Comparison of calculated and experimental data by penetration depth and weld width [9]

Modulation frequency, kHz	Penetration depth, mm		Weld width, mm	
	Experiment	Calculation	Experiment	Calculation
0	2.47	2.45	7.61	7.6
20	2.81	2.78	7.13	7.14
40	2.90	2.91	6.80	6.84
60	3.0	3.0	6.5	6.6
80	3.33	3.32	6.11	6.16

Table 14. Composition of material being welded (wt.%) [10]

Al	V	N	C	H	O	Fe	Ti
5.82	3.99	0.023	1.83	0.0007	0.063	<0.05	Bal.

sults of modeling together with the respective experimental data. Comparison of calculated and experimental data is indicative of their amazing coincidence (with the accuracy of the order of 1 %).

Work [10] of Chinese scientists is devoted to experimental study of the impact of frequency of pulse modulation of arc current on metal penetration in TIG welding. Experiments were performed using 3 mm arc with refractory (W + 2 % Ce) cathode of 2.4 mm diameter, shielding gas Ar (99.99 %) and welding speed of 150 mm/min. Samples 2.5 mm thick from titanium alloy TS4 were welded. Its composition is given in Table 14. Current modulation parameters were as follows: rectangular pulses in the form of a meander, repeated with the frequency in the range of

20–80 kHz, at base value of current $I_b = 40$ A, peak value $I_p = 100$ A (mean current of 70 A). Experiments on welding at direct current $I = 80$ A were conducted for comparison.

Dependencies of penetration depth H , weld width from sample face side B and weld form factor $\psi = H/B$ on modulation frequency f are given in Figure 15. As follows from experimental data presented in this Figure, weld width decreases markedly with increase of modulation frequency at a certain increase of penetration depth. The authors of [10] explain this tendency by reduction of the radius of anode binding of («root») r of the arc with increase of modulation frequency that is illustrated by experimental data given in Figure 16.

Work [11] is an experimental study of the impact of current parameters of LFP modulation in TIG welding of SAE 1020 steel 6.5 mm thick in argon atmosphere. Refractory cathode EWTh2 of 2.4 mm diameter with 60° sharpening angle of the working end was used. Arc length was 2 mm in all the experiments, welding speed was 10 cm/min. Arc current was modulated by rectangular pulses in the form of a meander repeated with the frequency of 50 Hz. Modulation current parameters are given in Table 15.

Figure 17 presents the experimental data on penetration depth, weld width and its cross-sectional area for the first seven experiments, which were performed while maintaining a constant mean value of arc current $I_m = 150$.

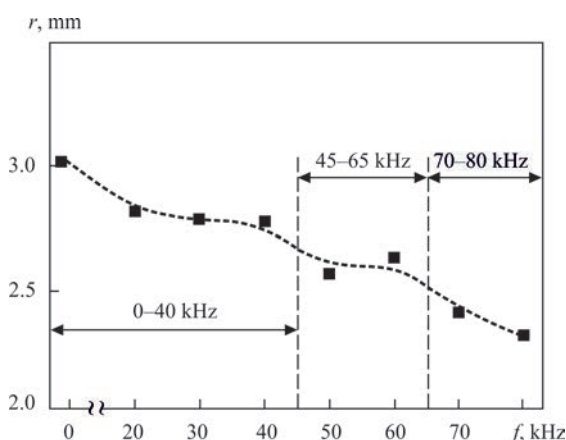


Figure 16. Dependence of arc root radius r on current modulation frequency f [10]

Table 15. Current parameters of modulation, used during experiment performance [11]

Experiment number	Base current value, A	Peak current value, A	Modulation amplitude, A	Mean current value, A		Effective current value, A	
				Calculation	Experiment	Calculation	Experiment
1	150	150	0	150	150	150	150
2	95	205	110	150	151	160	160
3	70	230	160	150	151	170	169
4	50	250	200	150	150	180	179
5	35	265	230	150	151	189	188
6	20	280	260	150	146	198	192
7	10	290	280	150	146	205	198
8	128	168	40	148	148	150	150
9	78	198	120	138	139	150	151
10	10	212	200	111	114	150	150

As follows from the diagrams given in this Figure, weld width increases with increase of modulation amplitude, and, therefore, of the effective (rms) value of current I_{rms} (see Table 15), while the penetration depth practically does not change, remaining below the respective value for DC welding. The cross-sectional area of the welds is also becoming larger with increase of effective value of current and begins exceeding the penetration depth in the case of DC welding at $I_{rms} > 198$ A.

Figure 18 gives similar data for experiments 1, 8–10, performed under the condition of constant I_{rms} and respective lowering of I_m .

The experimental data given in Figure 18 are indicative of noticeable reduction (compared to the respective DC welding characteristics) of penetration depth and cross-sectional area of the weld at decrease of mean value of arc current, whereas weld width does not change significantly. This led the authors of [11] to the conclusion that the penetration depth in TIG welding with low-frequency modulation of current depends mainly on mean value of modulated current, whereas weld width depends on its effective value.

Work [12] is also devoted to analysis of the impact of such characteristics of welding current modulation as its mean I_m and effective (rms) value I_{rms} on penetration depth, width and cross-sectional area of the weld, as well as on the rate of energy input in TIG welding of carbon steel 6.3 mm thick in argon atmosphere. Experiments were performed using a refractory cathode (W + 2 % Th) of 4 mm diameter with 60° angle of sharpening of the working end, arc length was constant, and equal to 3.5 mm, welding speed was 12 cm/min. Arc current was modulated by rectangular pulses in the form of a meander ($t_p = t_b = 0.25$ s, 2 Hz frequency), modulation current parameters are given in Table 16.

Experimental data given in Figure 19 confirm the conclusion of work [11] that the geometrical characteristics of welds in TIG welding of carbon steel with

LFP modulation of current are determined by both the mean and effective value of modulated current.

Analysis of the results of experimental work on investigation of the processes of metal penetration, geometrical characteristics, quality and mechanical characteristics of welds in TIG welding with welding current modulation leads to the following conclusions:

1. In TIG welding of aluminium alloys application of low-frequency pulse modulation of arc current with

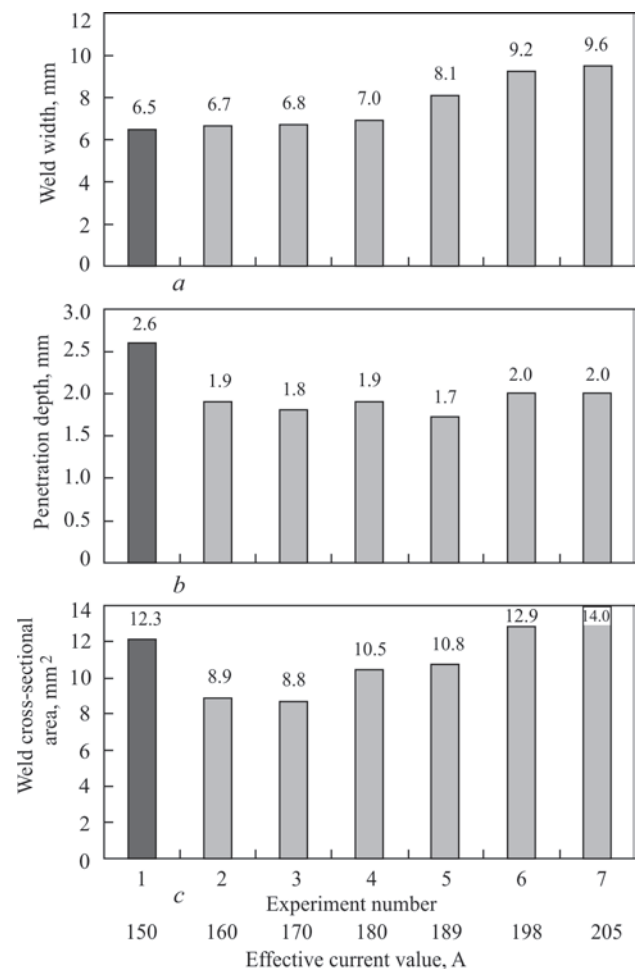


Figure 17. Dependencies of weld width (a), penetration depth (b) and weld cross-sectional area (c) on effective value of current at constant $I_m = 150$ A [11]

Table 16. Current modulation parameters used during the experiments [12]

Mode	Set parameters			Measured parameters			
	I_m, A	I_p, A	I_b, A	I_m, A	I_{rms}, A	U_m, V	U_{ms}, V
ΔI 300	200	350	50	199	249	12.5	12.8
ΔI 200	200	300	100	202	225	12.9	13.0
ΔI 100	200	250	150	200	206	12.7	12.9
ΔI 50	200	225	175	200	201	12.8	13.0
ΔI 20	200	210	190	200	200	12.6	12.8
ΔI 10	200	205	195	198	200	12.5	12.7
ΔI 0	200	–	–	199	200	12.8	12.8
ΔI 0	206	–	–	206	206	12.9	12.9
ΔI 0	224	–	–	225	225	12.6	12.6
ΔI 0	249	–	–	251	251	12.9	12.9

6 Hz frequency results in a noticeable improvement of strength properties (by 10–13 %), and increase of microhardness (up to 12 %) of weld metal, as well as lowering of residual stresses (up to 20 %), compared to samples, welded at direct current. This is caused by refinement of the structure of weld and HAZ metal at LFP modulation of welding current. Application of HFP modulation of current with the frequency of up to 25 kHz essentially reduces the number of pores and

nonmetallic inclusions per a unit of weld length (up to 80 %). In addition, such a modulation can be effectively used for breaking up the heterogeneous cast structure of weld metal, observed in the welds made at direct current. As a result, the microstructure of weld metal in TIG welding of aluminium alloys with HFP modulation of arc current is more homogeneous, so that such welds have fracture toughness values by 10–15 % higher than in DC welding.

2. In the case of TIG welding of stainless steel with low-frequency modulation of current by rectangular pulses repeated at the frequency of 1–5 Hz, the penetration depth and its ratio to weld width, turn out to be larger than in the case of DC welding with the same rate of energy input. At medium frequency sinusoidal

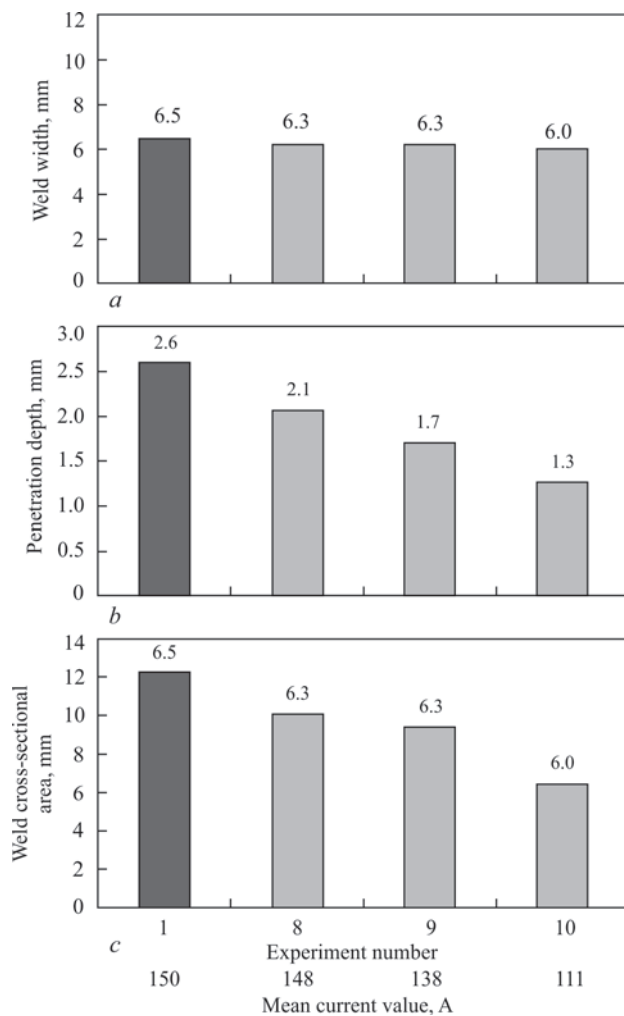


Figure 18. Dependencies of weld width (a), penetration depth (b) and weld cross-sectional area (c) on mean value of current at constant $I_{ms} = 150 A$ [11]

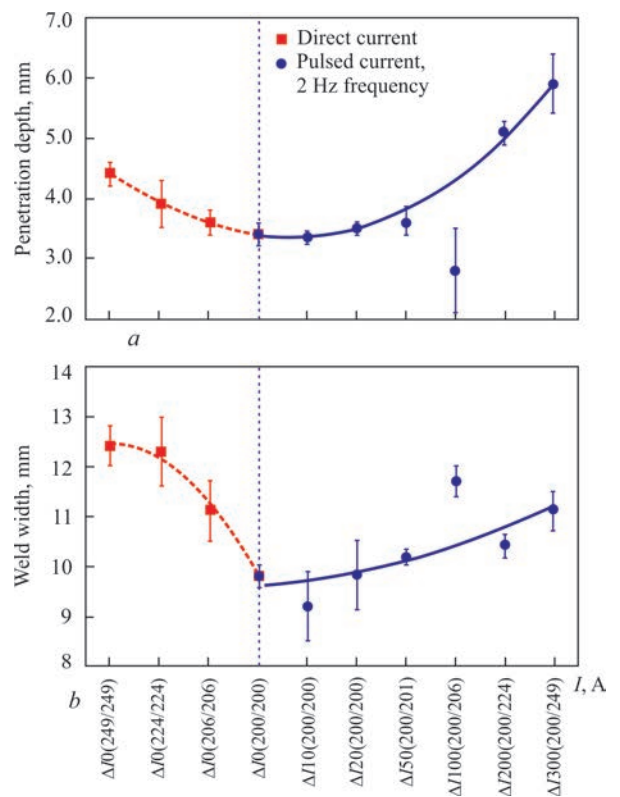


Figure 19. Impact of mean I_m and effective I_{rms} current values on penetration depth (a) and weld width (b), where ΔI is the modulation amplitude; in parenthesis — I_m/I_{rms} [12]

modulation of current in the range of up to 4 kHz and high-frequency modulation of current by rectangular pulses at frequencies in the range of 10–80 kHz, the penetration depth of stainless steel also exceeds the respective value at DC TIG welding, equal to mean value of modulated current. As regards the weld width, it turns out to be somewhat larger than the respective value for welds made by DC TIG welding.

3. With increase of frequency of pulse modulation of welding current in the case of TIG welding of nickel-chromium high-temperature alloys the size of the metal penetration zone decreases, whereas the size of HAZ increases. This is indicative of lowering of the efficiency of melting of the metal being welded (thermal efficiency) at increase of arc current modulation frequency. As regards the weld metal microstructure, application of HFP modulation of current does not lead to its noticeable improvement, compared to DC TIG welding.

4. At TIG welding of carbon steel with low-frequency modulation of current by rectangular pulses, the metal penetration depth mainly depends on mean value of modulated current, whereas the weld width depends on its effective value.

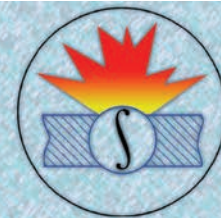
1. Boyi, U., Krivtun, I.V. (2019) Processes of nonconsumable electrode welding with welding current modulation (Review). Pt 1: Peculiarities of burning of nonstationary arcs with refractory cathode. *The Paton Welding J.*, **11**, 23–32.
2. Roden, W.A. (1972) High-frequency, pulsed-current GTA welding. In: *Proc. of National Aerospace Engineering and Manufacturing Meeting (2–5 Oct. 1972, San Diego, California, USA)*. Paper 720874, 1–8.
3. Leitner, R.E., McElhinney, G.H., Pruitt, E.L. (1973) An investigation of pulsed GTA welding variables. *Welding J., Res. Suppl.*, **9**, 405–410.
4. Omar, A.A., Lundin, C.D. (1979) Pulsed plasma — pulsed GTA arcs: A study of the process variables. *Ibid.*, **4**, 97–105.
5. Saedi, H.R., Unkel, W. (1988) Arc and weld pool behavior for pulsed current GTAW. *Ibid.*, **11**, 247–255.
6. Dzelnitzki, D. (2000) Muendersbach TIG — direct-current welding with high-frequency pulses, an interesting process variant. *EWM Hightec Welding GmbH*. WM008801. DOC: 08.00.
7. Onuki, J., Anazawa, Y., Nihei, M. et al. (2002) Development of a new high-frequency, high-peak current power source for high constricted arc formation. *Japan. J. Appl. Phys.*, **41**, 5821–5826.
8. Karunakaran, N., Balasubramanian, V. (2011) Effect of pulsed current on temperature distribution, weld bead profiles and characteristics of gas tungsten arc welded aluminum alloy joints. *Transact. Nonferrous Met. Soc. China*, **21**, 278–286.
9. Qi, B., Yang, M., Cong, B. et al. (2013) The effect of arc behavior on weld geometry by high-frequency pulse GTAW process with 0Cr18Ni9Ti stainless steel. *Int. J. Adv. Manuf. Technol.*, **66**, 1545–1553.
10. Yang, Z., Qi, B., Cong, B. et al. (2013) Effect of pulse frequency on weld appearance behavior by TC4 titanium alloys. *Transact. China Welding Institute*, **34**(12), 37–40.
11. Cunha, T.V.D., Louise-Voigt, A., Bohorquez, C.E.N. (2016) Analysis of mean and RMS current welding in the pulsed TIG welding process. *J. of Materials Processing Technology*, **231**, 449–455.
12. Silva, D.C.C., Scotti, A. (2016) Using either mean or RMS values to represent current in modeling of arc welding bead geometries. *Ibid.*, **240**, 382–387.

Received 04.11.2019

The Tenth International Conference Technologies in Welding and Related Mathematical Modeling and Information Processes

Dedicated to the 150th anniversary of the acad. E.O. Paton
– founder of the world's first welding institute

Ukraine, Odessa, Hotel «Arkadia»
September 14 – 18, 2020



The National Academy of Sciences of Ukraine
The E.O. Paton Electric Welding Institute
International Association «Welding»

To participate in the Conference, it is necessary to fill the Registration Form and send it to the Organizing Committee before June 19, 2020

Collections of proceedings of eight previous conferences «Mathematical Modelling and Information Technologies in Welding and Related Processes» on the site <http://patonpublishinghouse.com/eng/proceedings>

Deadlines

Registration form and Abstracts	Before 19 June, 2020
Second call for papers and confirmation of participation	Before 17 July, 2020
Payment of Registration Fee	Before 15 September, 2020

Organizing Committee

E. O. Paton Electric Welding Institute of NASU
11, Kazimir Malevich Str., Kyiv, 03150, Ukraine
Tel./Fax: (38044) 200-82-77; 205-22-26
E-mail: journal@paton.kiev.ua
<http://pwi-scientists.com/eng/mmi2020>